npj | climate and atmospheric science

www.nature.com/npjclimatsci

ARTICLE OPEN

Check for updates

Impacts of the North Atlantic biases on the upper troposphere/lower stratosphere over the extratropical North Pacific

Rajat Joshi [1]✉ and Rong Zhang [1,2]✉

The winter upper troposphere/lower stratosphere temperature/vertical motion response over the extratropical North Pacific induced by North Atlantic changes is not well understood. Here, using robust diagnostic calculations conducted in a fully coupled high-resolution climate model, we correct the North Atlantic ocean circulation biases and show that during wintertime, the North Atlantic cold surface temperature biases lead to a warmer upper troposphere/lower stratosphere over the extratropical North Pacific. In the upper troposphere/lower stratosphere over the extratropical North Pacific, this winter warming temperature response is linked to the vertical motion response through a simple leading order thermodynamic relationship between changes in the horizontal advection and adiabatic heating. The upper troposphere/lower stratosphere vertical motion response, which is also associated with the North Atlantic induced Walker circulation response over the tropical North Pacific, can provide a rough estimation of the upper troposphere/lower stratosphere warming response over the extratropical North Pacific.

npj Climate and Atmospheric Science (2023)6:151 ; https://doi.org/10.1038/s41612-023-00482-4

INTRODUCTION

The North Atlantic ocean is crucial for many regional climate phenomena through its linkage with the Atlantic Meridional Overturning Circulation (AMOC) and associated ocean heat transport[1–6]. Changes in the surface heat flux released from the North Atlantic to the atmosphere are important for the North Atlantic induced in-phase changes in the northern hemisphere mean surface temperature[7,8]. During winters, the North Atlantic sea surface temperature (SST) and associated air-sea heat flux changes can induce mid-latitude lower tropospheric temperature anomaly, which is advected over the north hemisphere by the mean jet stream and influences the low-level meridional eddy heat flux and storm tracks both locally and remotely over the North Pacific, and affect the North Pacific climate through atmospheric teleconnections amplified by coupled air-sea interactions[9]. Particularly, the North Atlantic induced tropospheric circulation changes over the extratropical North Pacific at the mid-tropospheric level resemble the Pacific North American (PNA[10]) like pattern[9,11]. The PNA and associated changes in the jet stream is shown to have a significant influence on weather and climate (temperature, precipitation) and mountain snowpack across the western United States[12,13]. The winter North Pacific SST response to the North Atlantic SST changes through both extratropical and tropical pathways[9,11,14,15] also resembles the Pacific Decadal Oscillation (PDO[16–18]) pattern associated with the PNA. The Atlantic-Pacific teleconnection is consistent with the simulated impact of the AMOC changes over the North Pacific[19–22] .The North Atlantic SST changes can also lead to changes in the surface temperature and Walker circulation over the tropical Pacific[11,14,23–27], similar to that induced by AMOC changes[21,28]. Hence initializing the North Atlantic ocean states could provide prediction skills for changes in the tropical Pacific[29,30].

Over the extratropical North Pacific, the wintertime PDO-like basin-scale surface cooling is observed to be associated with a trough with warmer upper troposphere/lower stratosphere above colder middle and lower troposphere, and the vertical dipole temperature anomaly switches sign at ~300hPa[31]. Modelling studies suggest that the local winter North Pacific PDO-like SST anomaly can induce only about 1/3 of this response, and another 2/3 of the response has to be induced by some remote forcing[32]. We hypothesize that the North Atlantic ocean might serve as the remote forcing. Most previous studies on the Atlantic-Pacific teleconnection are focused on the horizontal circulation and associated SST/lower troposphere temperature response over the North Pacific[9–11,14,19–21,33–37]. The remote impacts of the North Atlantic ocean for a wintertime upper troposphere/lower stratosphere warming response associated with the PDO-like basin-scale surface cooling over the extratropical North Pacific have not been explored. The vertical level at which the dipole temperature change switches sign is also the vertical level of the maximum change in the geopotential height. Understanding the unexplored winter upper troposphere/lower stratosphere temperature response is important for understanding the maximum jet stream response over the extratropical North Pacific through the thermal wind relationship.

Climate models have been used as one important tool to study the remote impacts of the North Atlantic changes because of the limitation of available observational records. However, many climate models have severe cold SST biases in the North Atlantic, which have been linked to the simulated AMOC strength[38]. The AMOC simulated in most climate models is much shallower than that observed from the RAPID program[39,40]. Climate models with more realistic Nordic Seas overflows can simulate a deeper AMOC, which interacts with the bathymetry and thus leads to more realistic North Atlantic Current pathways, reducing the cold SST biases in the North Atlantic[41–43]. The cold SST biases in the North Atlantic not only have impacts over the local North Atlantic and surrounding European regions[44] but also induce the cold SST biases in the extratropical North Pacific through atmospheric teleconnections and coupled air-sea interactions[15]. Whether the North Atlantic ocean circulation biases and associated cold SST biases can induce a winter upper troposphere/lower stratosphere

[1]Program in Atmospheric and Oceanic Sciences, Princeton University, Princeton, NJ, USA. [2]NOAA/OAR/GFDL, Princeton, NJ, USA. ✉email: rajatjoshi@princeton.edu; rong.zhang@noaa.gov

warming response above the middle/lower tropospheric cooling response and, thus a vertical dipole temperature change over the extratropical North Pacific has not been investigated.

Previous observational and modelling studies have also found that the North Atlantic SST over the Gulf Stream region can affect local upper tropospheric vertical motion in summer[45–47]. However, the climatic influence of the open-ocean Gulf Stream pathway (after its separation from the US east coast) on atmospheric vertical motion is shallow and limited to the local lower and middle troposphere in winter[45]. It is unclear whether the North Atlantic ocean circulation biases and associated SST biases can have sustained influence on remote upper troposphere/lower stratosphere vertical motion over the extratropical North Pacific even if their climatic impacts on local tropospheric vertical motion over the North Atlantic are shallow in winter.

Here, we conduct robust diagnostic calculations (RDC) in a fully coupled high-resolution climate model to correct North Atlantic ocean circulation biases and assess the impacts of the North Atlantic biases on winter upper troposphere/lower stratosphere vertical motion and temperature changes over the extratropical North Pacific. The fully coupled high-resolution climate model used for the RDC experiments[48] is also employed to generate a corresponding present-day control simulation without correcting North Atlantic ocean circulation biases for comparison (see "Methods"). The RDC approach was first proposed by Sarmiento and Bryan[49] and has been used to study the ocean circulation in regional ocean-only models[49,50], a global ocean model coupled to an atmospheric energy balance model, and a slab sea ice model[51], a global ocean-ice coupled model[52,53], and a global fully coupled high-resolution climate model[54]. Here, the RDC approach is applied to study the ocean's role in the atmosphere.

In the RDC experiment used in this study, the North Atlantic potential temperature and salinity in the coupled model are restored to the observed hydrographic climatology in the entire ocean column to produce a realistic North Atlantic ocean circulation, thus correcting the North Atlantic ocean circulation and associated SST biases (see "Methods"). The long-term mean difference between the control and RDC experiments (Control minus RDC) is used to assess the influence of the North Atlantic biases on winter upper troposphere/lower stratosphere vertical motion and temperature changes over the extratropical North Pacific. Our results suggest that the North Atlantic ocean circulation and associated cold SST biases can lead to a wintertime upper troposphere/lower stratosphere warming response over the extratropical North Pacific. The winter upper troposphere/lower stratosphere warming response is linked to the upper troposphere/lower stratosphere vertical motion response over the extratropical North Pacific through a simple leading order thermodynamic relationship between changes in the horizontal advection and adiabatic heating. A better understanding of the winter upper troposphere/lower stratosphere temperature changes over the extratropical North Pacific in response to changes in the North Atlantic Ocean is of great importance in understanding the associated winter maximum jet stream response over the extratropical North Pacific, which has significant socioeconomic impacts.

RESULTS

Winter atmospheric changes over the extratropical North Pacific in response to the North Atlantic biases

Compared to the RDC, the North Atlantic SST in the control simulation is much colder (Fig. 1a, d), which has been found in many climate models. The colder mid-latitude North Atlantic SST in the control simulation is associated with the unrealistic eastward shift of the North Atlantic Current (NAC) (Fig. 1a, d) due to deficiencies in simulated Nordic Sea overflows and downstream deep western boundary current (DWBC; Fig. 1b, e)[43]. In the control simulation, the southward moving deep branch of the AMOC is weaker and shallower compared to that in the RDC (Fig. 1b, c, e, f), and hence the simulated NAC not only shifts eastward but is also weaker in strength and much shallower (Fig. 1c, f)[43]. The deep ocean is much warmer in the control simulation due to the lack of cold dense Nordic Sea overflows and associated DWBC (Fig. 1b, e). The RDC approach generates a consistent ocean density field, which produces a realistic North Atlantic ocean circulation and effectively corrects the North Atlantic ocean circulation and associated temperature biases presented in the control simulation[54].

We also conduct the SST nudging experiment, in which only the North Atlantic SST in the coupled model is restored to the observed climatological data (see "Methods"). In the SST nudging experiment (Supplementary Fig. 1g-i), although the North Atlantic cold SST biases are reduced compared to the control simulation, the North Atlantic ocean circulation biases remain uncorrected. The deep branch of AMOC remains shallower and weaker, and the NAC pathway remains unrealistic (Supplementary Fig. 1h, i). Hence, substantial North Atlantic cold SST biases persist in the SST nudging experiment, unlike the RDC experiment (Supplementary Fig. S2). Both the SST nudging experiment and the control simulation have unrealistic strong cyclonic subpolar gyre (Supplementary Fig. 1d, g) associated with unrealistic strong Labrador Sea deep convection[54]. Since the cold SST biases east of Flemish Cap are reduced in the SST nudging experiment compared to the control simulation, relatively warmer SST is advected by the unrealistic strong subpolar cyclonic gyre, resulting in even larger warm SST biases around the rim of the subpolar North Atlantic and associated larger warm temperature biases in the deep North Atlantic (Supplementary Figs. 1h, 2a) than those in the control simulation. The RDC-derived climatological winter net downward surface heat flux matches well with the observations, and has strong heat released from the ocean into the atmosphere along the Gulf Stream and the NAC (Supplementary Fig. 3a, b) due to a realistic representation of the North Atlantic ocean circulation. In contrast, the SST nudging experiment and the control simulation lack strong ocean heat release east of Flemish Cap, indicating an unrealistic NAC pathway (Supplementary Fig. 3c, d). Overall, the SST nudging experiment does not produce a realistic North Atlantic ocean circulation as the RDC experiment, hence does not effectively correct the North Atlantic cold SST biases.

The wintertime (Jan through March; JFM) response to the North Atlantic biases (Control minus RDC) is not only local but is also evident in remote regions (Fig. 2). Outside of the North Atlantic, there is a surface cooling response (in both the surface air temperature and SST), particularly over the mid-latitude North Pacific (Fig. 2a and Supplementary Fig. 4a). This is consistent with previous studies suggesting that on longer timescales, the North Pacific PDO-like SST changes are affected by the North Atlantic SST changes initially through atmospheric pathways and subsequently reinforced by regional ocean dynamics and coupled air-sea interactions[7,9,11,15]. Associated with the changes in surface temperature and thus spatial surface temperature gradients, there is a southward shift in the near-surface meridional transient eddy heat flux ($\overline{v'T'}$), indicating a southward shift of the winter storm track over both the North Atlantic and the North Pacific (Fig. 2b). The imprint of the shift in the storm track is seen in the changes in the winter northern hemisphere large-scale extreme (the 95th percentile) precipitation (Fig. 2c). The regions with enhanced extreme precipitation over the United States, East Asia, North Pacific, and North Atlantic often coincide with the regions with enhanced meridional transient eddy heat flux (Fig. 2b, c). In comparison to the RDC, there is a significant increase (~30–40% increase; Supplementary Fig. 4c) in the large-scale extreme precipitation in the control simulation over the western United

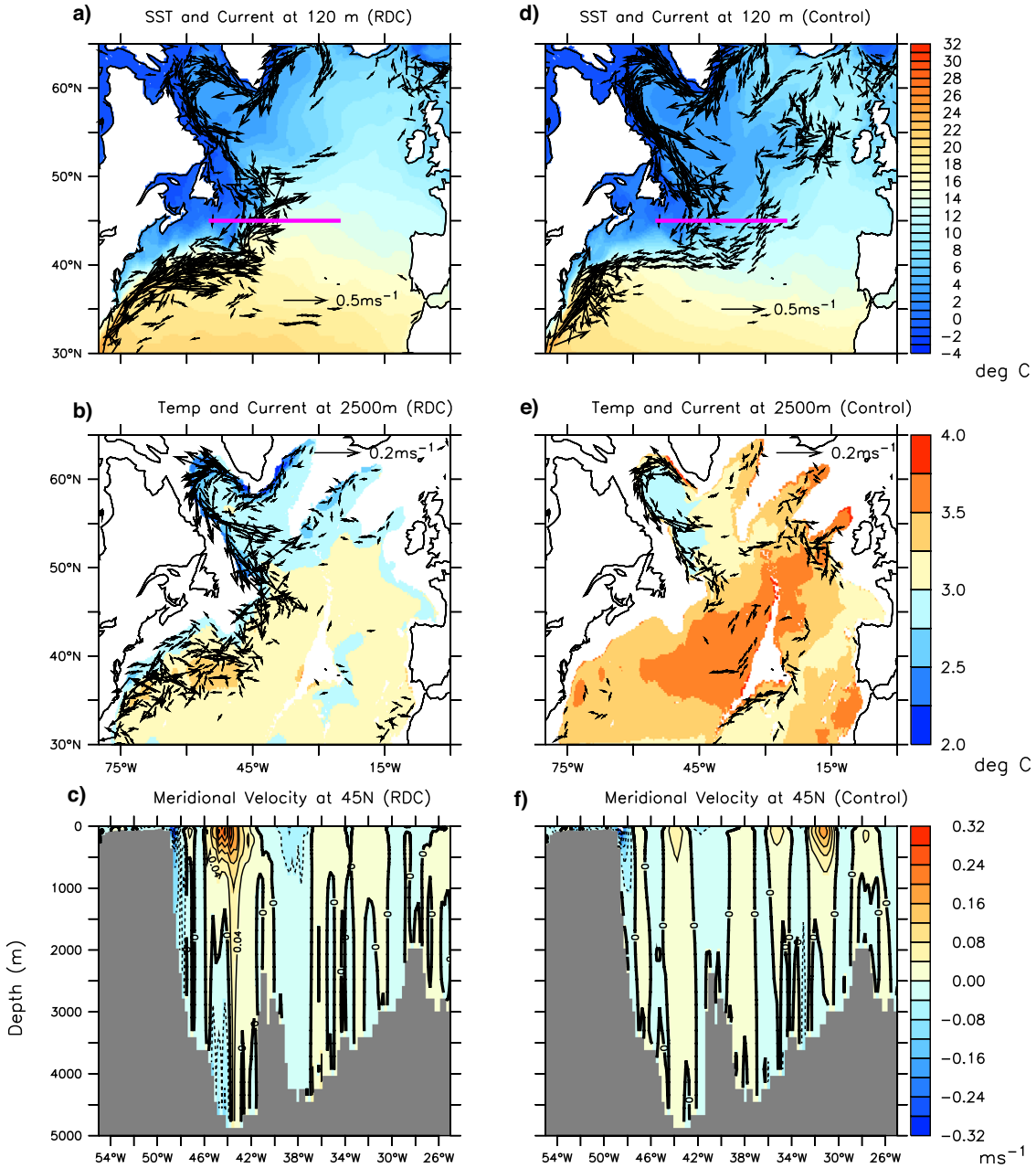

Fig. 1 Mean winter (JFM) SST, deep ocean temperature, and ocean circulation in the North Atlantic. a SST in °C as shading and ocean currents (ms^{-1}) at 120 m depth as vectors (vectors smaller than 0.08 ms^{-1} in magnitude are not shown) from RDC. **b** Deep ocean (2500 m) temperature as shading and ocean currents as vectors (vectors smaller than 0.02 ms^{-1} in magnitude are not shown) from RDC. **c** Meridional ocean velocity at section 45°N (magenta line in panel **a**) in ms^{-1} from RDC, contour interval is 0.04 ms^{-1}. **d**–**f** as **a**–**c** but for the control experiment.

States, suggesting the profound remote societal impact that changes in the North Atlantic ocean circulation could have.

The North Atlantic biases also induce a southward shift of the winter Inter-Tropical Convergence Zone (ITCZ) over both the tropical Atlantic and the eastern tropical Pacific, and thus a strengthened Walker circulation over the central and western tropical North Pacific (Fig. 2d), similar to the pattern of the tropical precipitation response induced by the AMOC weakening[21]. The southward ITCZ shift is accompanied by more northeasterly surface winds along the eastern tropical Pacific coast (Supplementary Fig. 5a). These northeasterly surface winds cause more upwelling of subsurface cold ocean water, resulting in colder SST in the eastern tropical Pacific north of equator (Supplementary Fig. 4a), which strengthens the Walker circulation over the central and western tropical North Pacific as reflected in the surface wind stress change over this region (Supplementary Fig. 5a). Here the mechanism for the North Atlantic-induced Walker circulation change is consistent with the mechanism of the southward ITCZ shift and associated strengthened Walker circulation over the tropical North Pacific in response to the AMOC weakening[21].

Additionally, the North Atlantic-induced Walker circulation response can be further confirmed by results compared to the SST Nudging experiment that does not effectively correct the North Atlantic cold SST biases. The difference between the Control and SST Nudging experiments underestimates the North Atlantic cold SST biases, and the impacts of the underestimated North

Atlantic cold SST biases can be seen in the precipitation response (Supplementary Fig. 6a, d). Although the precipitation response pattern is similar to that between the Control and RDC experiments, both the North Atlantic-induced ITCZ shift and Walker circulation change are weaker between the Control and SST Nudging experiments, compared to the difference between

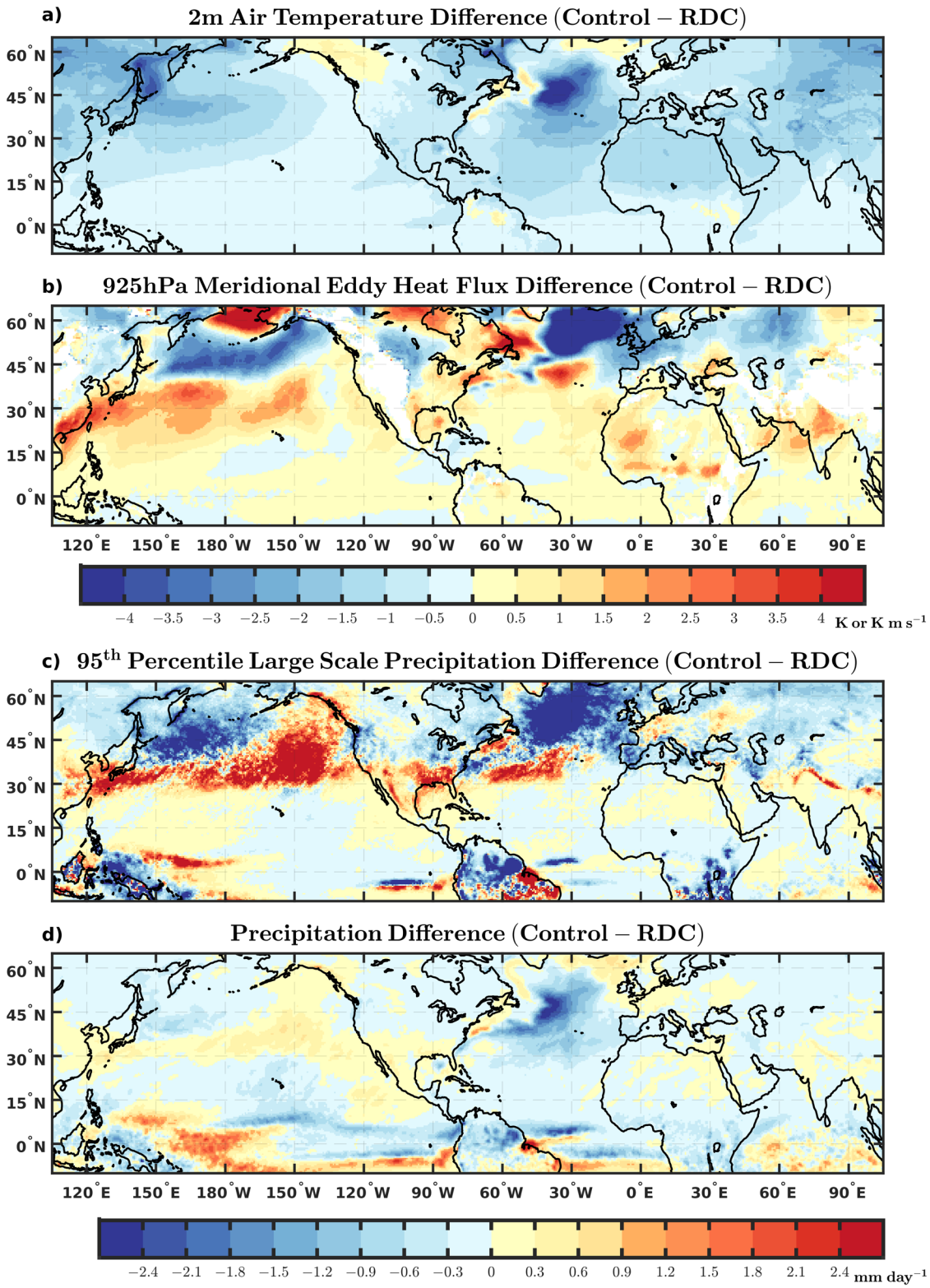

Fig. 2 Difference of wintertime (JFM) mean near surface air temperature, meridional eddy heat flux, extreme large-scale precipitation, and total precipitation between the Control and RDC experiments. a Surface 2-m air temperature (T_{2m}) in K. **b** Meridional eddy heat flux ($\overline{v'T'}$) in Kms^{-1} at 925 hPa. **c** The 95th percentile large-scale extreme precipitation (mm day^{-1}). **d** Total precipitation (large-scale plus convective) (mm day^{-1}).

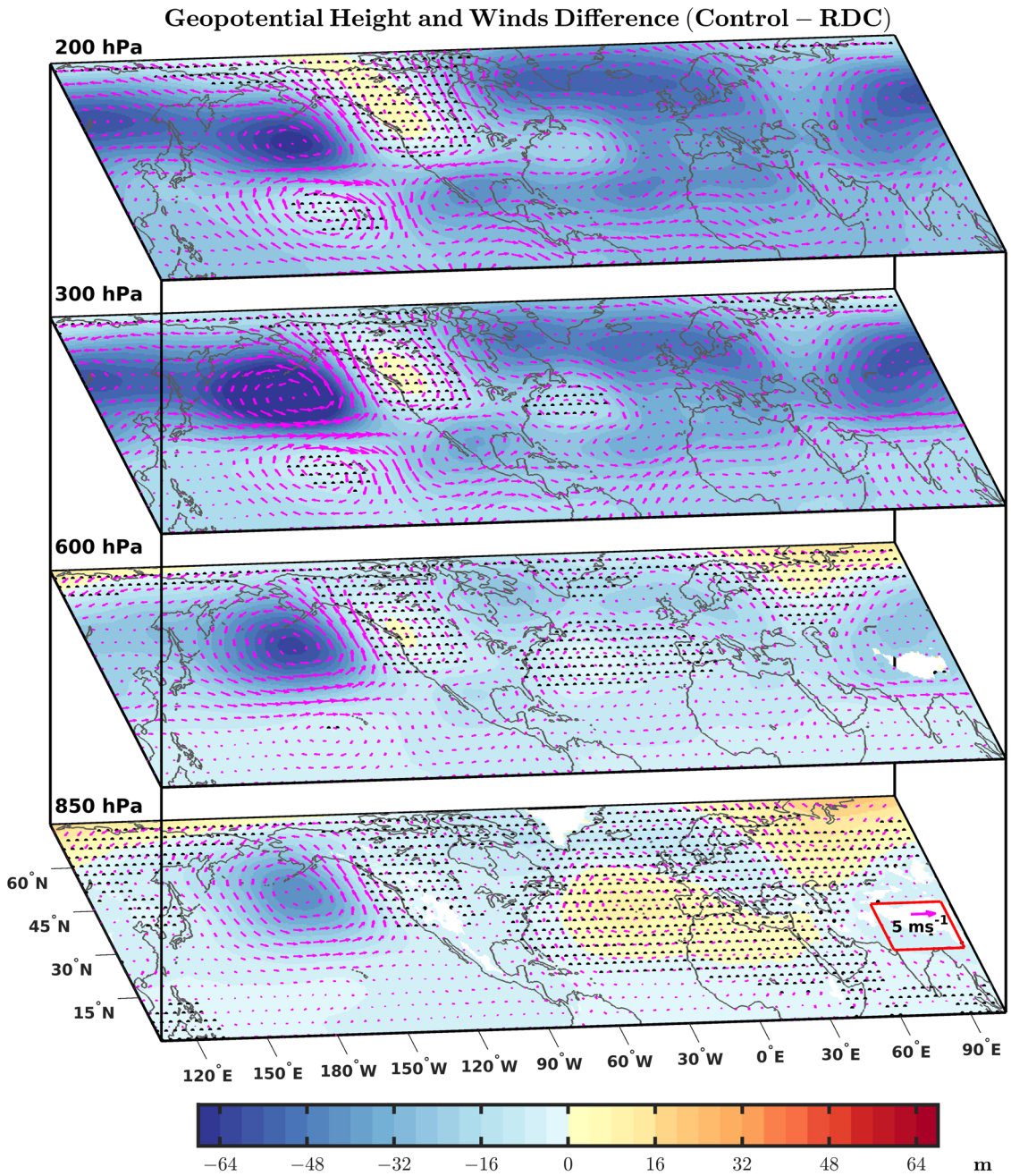

Fig. 3 Difference of winter (JFM) mean geopotential height and wind between the Control and RDC experiments at different levels. The geopotential height (wind) is represented as shading (vector) in m (ms^{-1}). Stippling (black color) indicates the regions where geopotential height differences are not significant at 5% level.

the Control and RDC experiments (Supplementary Fig. 6a, d). The weaker ITCZ shift and hence the weaker Walker circulation change in response to the underestimated North Atlantic cold SST biases confirms the crucial role of the North Atlantic cold SST biases in inducing these responses.

The winter atmospheric response over the extratropical North Pacific to the North Atlantic biases is associated with an enhanced cyclonic circulation with a PNA-like pattern (Fig. 3). The spatial pattern of the cyclonic circulation response here over colder North Pacific SST is similar to that associated with the observed PDO[31,32]. The North Atlantic cold biases and associated reduced surface turbulent heat fluxes (Supplementary Fig. 4b) induce near-surface cooling, which is advected eastward by the mean jet stream, leading to near-surface cooling over the Northern Hemisphere (Fig. 2a). Compared to the RDC, the control simulation has colder winter temperatures at low levels over most regions in the Northern Hemisphere (Fig. 4), consistent with previous studies showing that ocean-triggered multidecadal North Atlantic SST changes can lead to in-phase Northern Hemisphere mean surface temperature changes through atmospheric pathways[7,8]. Over the extratropical North Pacific, the North Atlantic-induced near-surface cooling leads to southward shifts in storm tracks (Fig. 2b), and thus a southward shift in the westerly surface wind and a strengthening in the Aleutian low, i.e., a low-level negative geopotential height anomaly over the region (Fig. 5a). This is consistent with the mechanism for the negative (positive) sea level pressure (SLP) response over the extratropical North Pacific induced by multidecadal North Atlantic cooling (warming)[9].

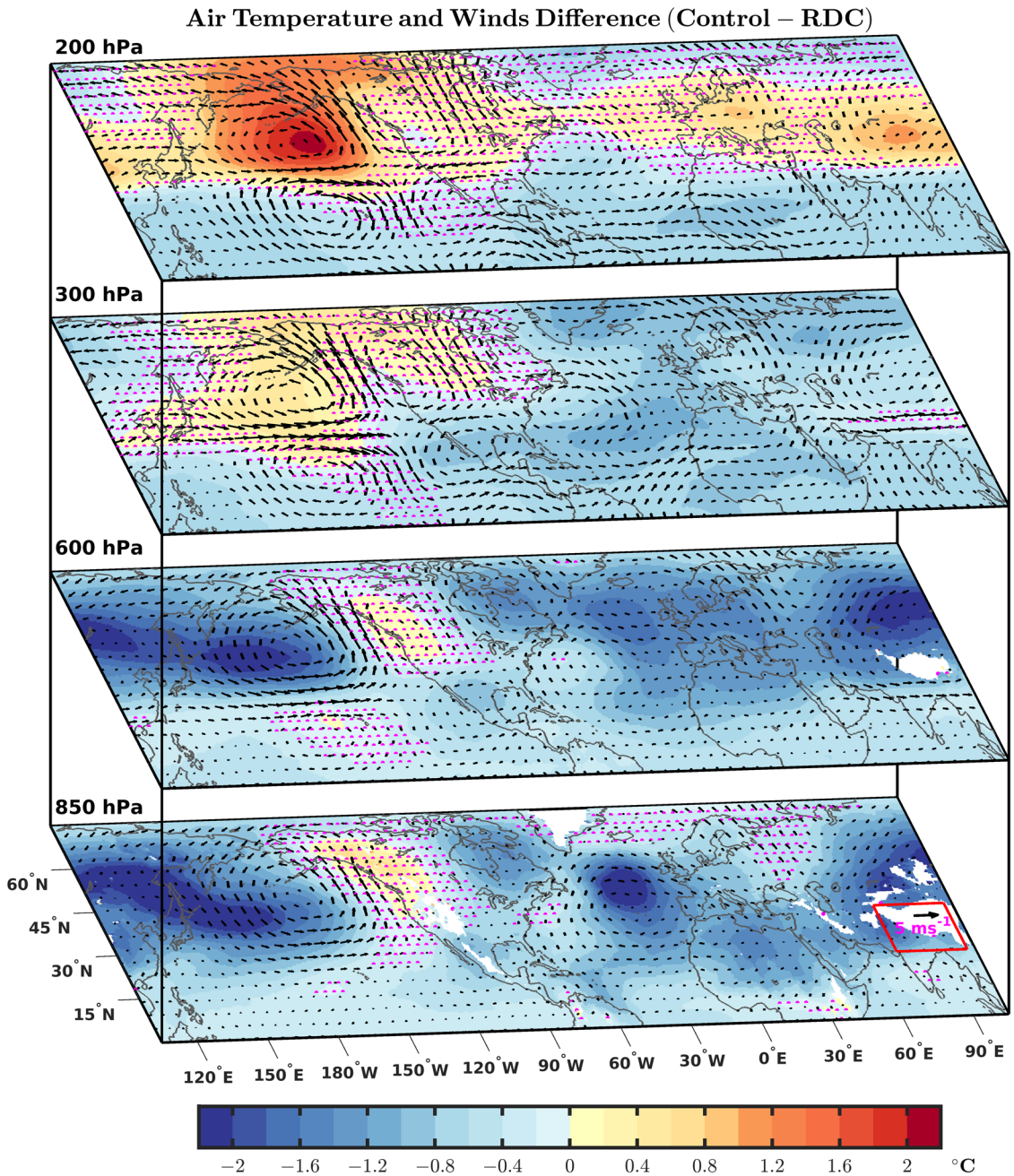

Fig. 4 Difference of winter (JFM) mean air temperature and wind between the Control and RDC experiments at different levels. Air temperature (wind) is represented as shading (vector) in °C (ms^{-1}). Stippling (magenta color) here indicates that air temperature differences are not significant at 5% level. Wind vectors here are as shown in Fig. 3.

Moving up in the atmosphere over the extratropical North Pacific, the cooling response is reduced, and the temperature response even switches sign into a warming response in the upper troposphere/lower stratosphere (Fig. 4). Notably, the vertical dipole atmospheric temperature response over the extratropical North Pacific is linked to the cyclonic circulation (Fig. 3). The zonal averaged atmospheric temperature and geopotential height response (Fig. 5a) over the extratropical North Pacific shows that the low geopotential height response increases vertically from the surface until 300hPa and then decreases, and the atmospheric temperature response switches sign from negative to positive at the level of the maximum low geopotential height response (300hPa). This switch in sign is consistent with the hydrostatic and thermal wind balance, and thus there are enhanced westerlies (easterlies) centered around 32°N (57°N) over the extratropical North Pacific with a maximum response at ~300hPa (Fig. 5b). Above the surface boundary layer (925hPa), the negative geopotential height response over the extratropical North Pacific can be deduced and understood from the air temperature response by the hypsometric equation ($dz = \frac{-R_d T}{g} d(lnp)$), obtained by combining the hydrostatic balance ($\frac{dp}{dz} = -\rho g$), (and ideal gas law ($p = \rho R_d T$). The calculated geopotential height response (Supplementary Fig. 7b, c) ($\Delta\overline{z}_p = \Delta\overline{z}_{925hPa} - \frac{R_d}{g}\int_{925hPa}^{p} \Delta\overline{T} d(lnp)$) over the extratropical North Pacific not only mirrors the structure but also matches the magnitude of the modeled geopotential height response, highlighting the importance of understanding the mechanisms that sustain the air temperature response over that region. Overall, the changes in

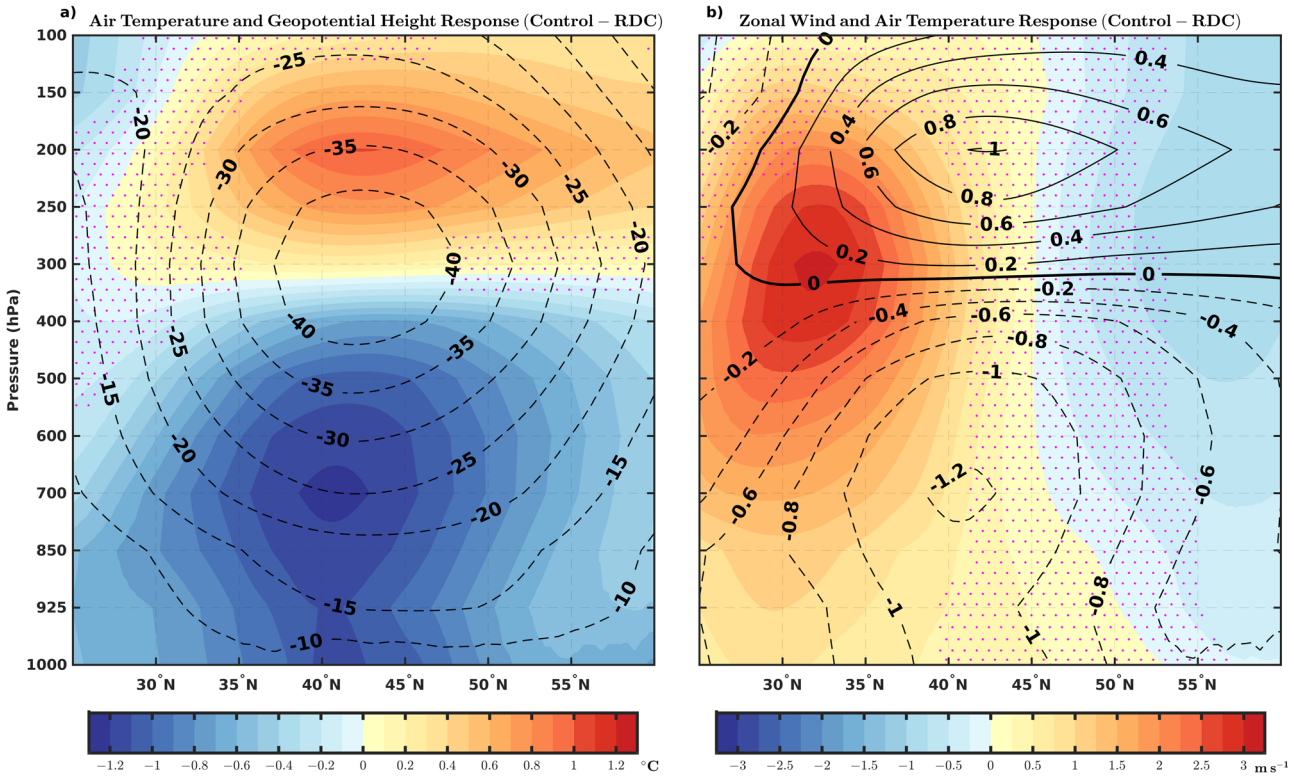

Fig. 5 Zonal averaged difference of wintertime (JFM) mean geopotential height, air temperature and zonal wind speed between Control and RDC experiments over the North Pacific. a Air temperature (geopotential height) in °C (m) is represented as shading (contour). **b** Zonal wind (air temperature) as shading (contour) in ms^{-1} (°C). In both (**a**) and (**b**) zonal averaging is done between 140 °E and 130°W. Stippling (magenta color) here indicates air temperature differences in (**a**) and zonal wind differences in (**b**) are not significant at 5% level.

zonal winds and associated cyclonic circulation response over the extratropical North Pacific are consistent with the vertical dipole atmospheric temperature response through the thermal wind relationship.

Our results here show that during wintertime, the North Atlantic biases not only induce a cooling in the lower and middle troposphere ($\Delta\overline{T}<0$) but also a warming in the upper troposphere/lower stratosphere ($\Delta\overline{T}>0$) over the extratropical North Pacific. The spatial pattern of the vertical dipole atmospheric temperature response (warming above cooling) over the colder western and central extratropical North Pacific is similar to that associated with the observed PDO, in which the vertical dipole atmospheric temperature anomaly also switches sign at ~300hPa[31,32].

In the upper troposphere/lower stratosphere over the extratropical North Pacific, there is also a significant response in winter vertical velocity ($\Delta\overline{\omega}$ in isobaric coordinate) (Fig. 6). In contrast, over the western extratropical North Atlantic, the winter vertical velocity response is mainly confined to the lower and middle troposphere, consistent with previous studies showing that the local climatic influence of the open-ocean Gulf Stream pathway on atmospheric vertical velocity above it is shallow and limited to the lower and middle troposphere in winter[45,47]. The enhanced sinking (rising) motion over the western (eastern) extratropical North Pacific (Fig. 6) is consistent with the enhanced upper-tropospheric/lower stratosphere convergence (divergence) of the winds (Supplementary Fig. 8a) at the southwestern (southeastern) side of the enhanced cyclonic circulation (Figs. 4, 5).

As discussed earlier, the North Atlantic biases also induce a southward shift of the winter ITCZ over both the tropical Atlantic and the eastern tropical Pacific and an enhanced Walker circulation north of the equator over the Pacific (Fig. 2d), similar to the pattern of the tropical response induced by the AMOC weakening[21]. Coupled air-sea interactions are important for the Atlantic-induced Walker circulation response over the tropical North Pacific[21]. The enhanced rising (sinking) motion and upper tropospheric divergence (convergence) over the western (eastern) tropical Pacific north of the equator are associated with the enhanced Walker circulation (Fig. 6, S8a). These changes contribute to a stronger (weaker) meridional flow centered around 20°N at 200hPa (Supplementary Fig. 9), and thus the enhanced convergence (divergence) (Supplementary Fig. 8a) and sinking (rising) motion (Fig. 6) at the southwestern (southeastern) side of the enhanced cyclonic circulation over the extratropical North Pacific. The impact of the strengthened Walker circulation becomes more evident in the velocity potential and the divergent winds at 200hPa (Supplementary Fig. 5b), where divergence (convergence) over the regions of enhanced (reduced) precipitation over the tropical North Pacific is associated with convergence (divergence) and thus sinking (rising) vertical motion over the western (eastern) extratropical North Pacific. In addition, these tropical ITCZ/Walker circulation responses over the tropical North Pacific also contribute to the enhanced anticyclonic circulation at 200hPa over the subtropical North Pacific (Figs. 4, 5).

Thermodynamic analysis of winter vertical dipole atmospheric temperature response over the extratropical North Pacific

We identify the mechanisms that sustain the winter vertical dipole atmospheric temperature response over the extratropical North Pacific through the thermodynamic equation. The thermodynamic analysis (see "Methods") gives an insight into the dominant processes for sustaining changes in atmospheric temperature at a particular location, similar to the approach used to study the vertical dipole atmospheric temperature anomaly over the Tibetan Plateau[55]. The spatial distribution of the dominant thermodynamic terms at 200hPa and 850hPa shows the leading order terms sustaining the winter upper troposphere/lower stratosphere and

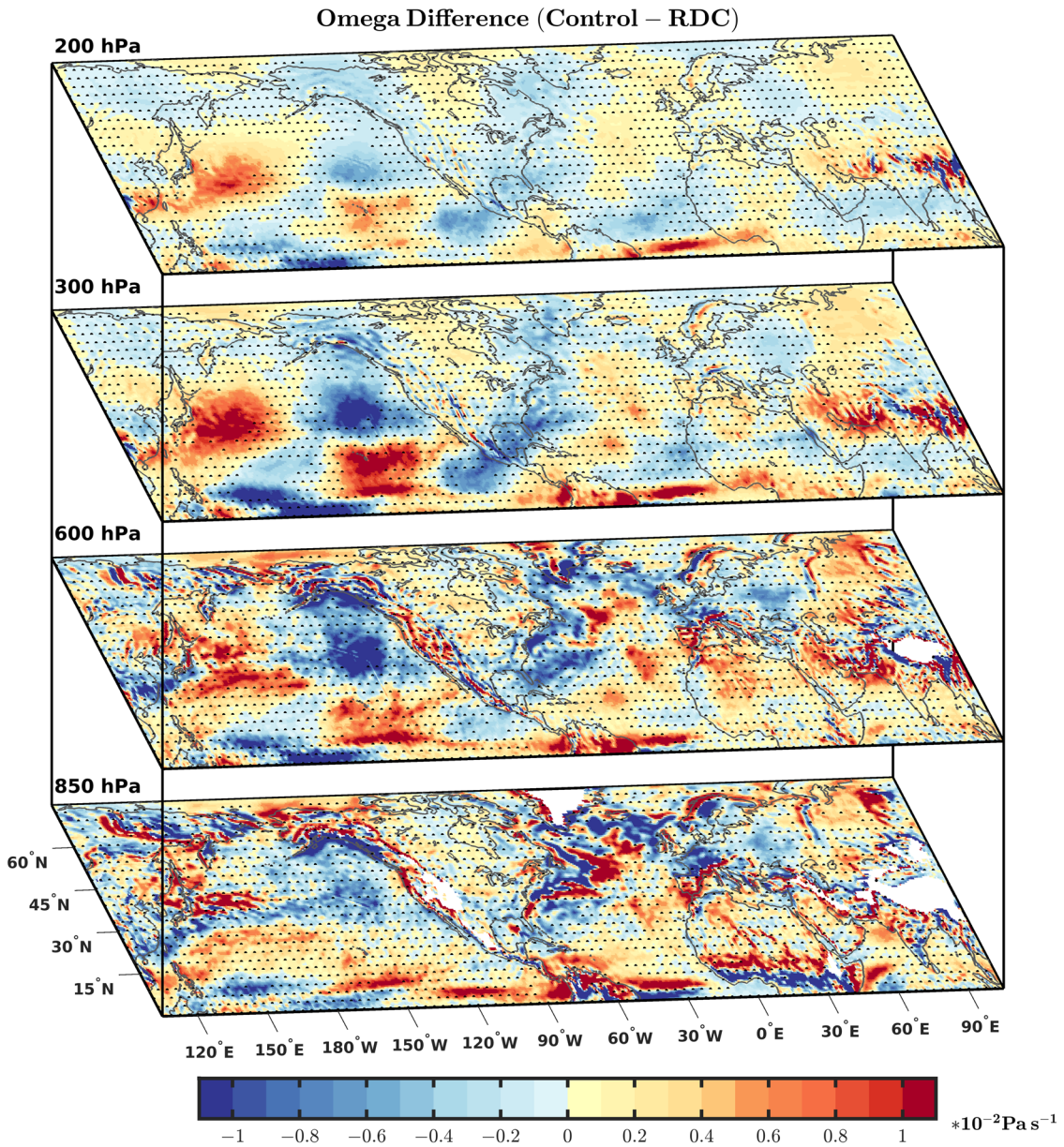

Fig. 6 Difference of winter (JFM) mean vertical velocity (x10^{-2}) in pressure coordinate (Pa s^{-1}) between the Control and RDC experiments at different levels. Stippling (black color) here represents the region where the vertical velocity differences are not significant at 5% level.

lower troposphere temperature response over the extratropical North Pacific respectively (Supplementary Fig. 10), the remaining terms in the thermodynamic equation at these levels are negligible.

In the upper troposphere/lower stratosphere at 200hPa, changes in the diabatic heating and eddy heat flux terms are negligible, and thus over the western extratropical North Pacific, the warming response is sustained by enhanced adiabatic heating and damped by reduced horizontal advection, whereas over the eastern extratropical North Pacific, the warming response is sustained by enhanced horizontal advection and damped by reduced adiabatic heating (Supplementary Fig. 10a, b). The decomposition of the total changes in horizontal advection and adiabatic heating in terms of changes in temperature and velocity (see "Methods") suggests that at 200hPa, the total change in the horizontal advection term in the thermodynamic equation is primarily dominated by the mean zonal flow advection of the temperature change $\left(-\overline{u}_{\mathrm{RDC}}\frac{\partial\Delta\overline{T}}{\partial x}\right)$ (Fig. 7a, Supplementary Fig. 10a). The contribution of other terms involving changes in temperature and winds to the total change in the horizontal advection term is negligible, which is related to the fact that the meridional mean flow $\overline{v}_{\mathrm{RDC}}$ is much smaller than the zonal mean flow $\overline{u}_{\mathrm{RDC}}$ and the horizontal gradients of the climatological temperature $\frac{\partial\overline{T}_{\mathrm{RDC}}}{\partial x}$ and $\frac{\partial\overline{T}_{\mathrm{RDC}}}{\partial y}$ are relatively small at 200hPa. Meanwhile, the total change in the adiabatic heating term in the thermodynamic equation at 200hPa is dominated by the change in the vertical velocity (i.e. $-\Delta\overline{\omega}\frac{\partial\overline{\theta}_{\mathrm{RDC}}}{\partial p}\left(\frac{p}{p_s}\right)^{\frac{R_d}{c_p}}$) (Fig. 7b, Supplementary Fig. 10b), since $\frac{\partial\overline{\theta}_{\mathrm{RDC}}}{\partial p}$ is relatively large at this level (mostly above the tropopause) over the extratropical North Pacific. Hence our thermodynamic analysis suggests a simple leading order relationship between the mean zonal flow advection of the temperature change $\left(-\overline{u}_{\mathrm{RDC}}\frac{\partial\Delta\overline{T}}{\partial x}\right)$ and

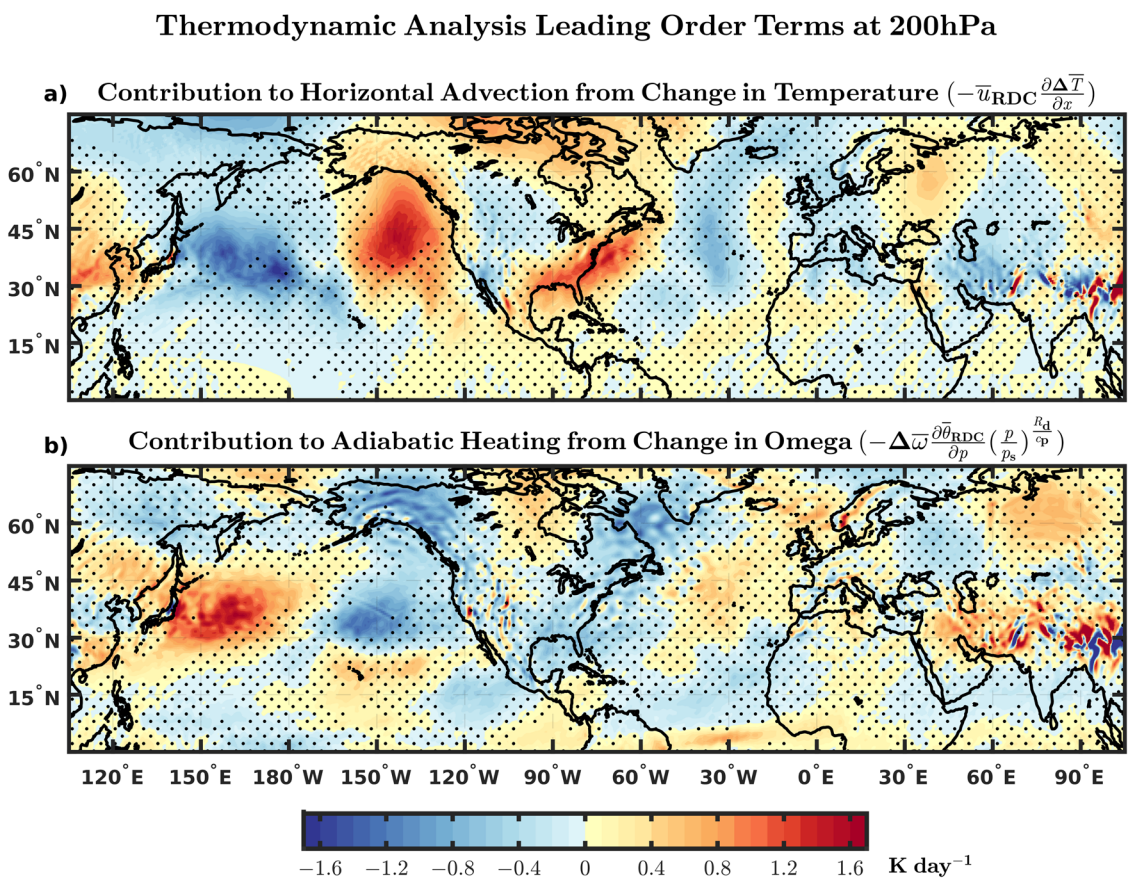

Fig. 7 Thermodynamic analysis leading order terms at 200 hPa. a Contribution of the mean zonal flow advection of the temperature change to the horizontal advection. **b** Contribution of the vertical advection of mean potential temperature by the change in omega to the adiabatic heating. Colorbar in K day^{-1}. Stippling (black color) here represents the region where differences are not significant at 5% level.

the vertical advection of the mean potential temperature by change in vertical velocity $(-\Delta\overline{\omega}\frac{\partial\overline{\theta}_{\mathrm{RDC}}}{\partial p}\left(\frac{p}{p_s}\right)^{\frac{R_d}{c_p}})$ at 200hPa over the extratropical North Pacific:

$$0 \approx -\overline{u}_{\mathrm{RDC}}\frac{\partial\Delta\overline{T}}{\partial x} - \Delta\overline{\omega}\frac{\partial\overline{\theta}_{\mathrm{RDC}}}{\partial p}\left(\frac{p}{p_s}\right)^{\frac{R_d}{c_p}} \quad (1)$$

$$\overline{u}_{\mathrm{RDC}}\frac{\partial\Delta\overline{T}}{\partial x} \approx -\Delta\overline{\omega}\frac{\partial\overline{\theta}_{\mathrm{RDC}}}{\partial p}\left(\frac{p}{p_s}\right)^{\frac{R_d}{c_p}} \quad (2)$$

This simple and powerful relationship between the leading horizontal advection and adiabatic heating terms can be used to roughly estimate the amplitude of the Atlantic-induced upper troposphere/lower stratosphere temperature response $\Delta\overline{T}_X$ at a given latitude and zonal distance (X) from the western boundary (X_{W}) over the extratropical North Pacific, if the vertical motion response $\Delta\overline{\omega}$ is given (along with the climatology of $\overline{u}_{\mathrm{RDC}}$ and $\frac{\partial\overline{\theta}_{\mathrm{RDC}}}{\partial p}$):

$$\Delta\overline{T}_X = \int_{X_{\mathrm{W}}}^{X} -\frac{\Delta\overline{\omega}}{\overline{u}_{\mathrm{RDC}}}\frac{\partial\overline{\theta}_{\mathrm{RDC}}}{\partial p}\left(\frac{p}{p_s}\right)^{\frac{R_d}{c_p}}dx + \Delta\overline{T}_{X_{\mathrm{W}}} \quad (3)$$

For example, over the western extratropical North Pacific around 40°N, if we consider the zonal length scale L of *~4260 km* (from 130°E to 180°E), $\overline{u}_{\mathrm{RDC}}$ as *~36* ms^{-1}, $-\Delta\overline{\omega}\frac{\partial\overline{\theta}_{\mathrm{RDC}}}{\partial p}\left(\frac{p}{p_s}\right)^{\frac{R_d}{c_p}}$ *as* $\sim 1.0K$day^{-1}, the roughly estimated temperature response $\Delta\overline{T}_X$ at 200hPa over the central extratropical North Pacific around 180°E is *~1.4 K* (neglecting the weak temperature response $\Delta\overline{T}_{X_{\mathrm{W}}}$ at the western edge around 130°E), similar to the simulated temperature difference between the Control and RDC experiments over the region. The adjustment time scale of the temperature response to the vertical motion change, which is also the zonal advective time scale, $\tau \sim \frac{L}{\overline{u}_{\mathrm{RDC}}}$, is very short (~1–2 days). As illustrated in the schematic diagram (Fig. 8), with an integrated increase in the upper level sinking vertical motion/adiabatic heating over the western extratropical North Pacific, the warm temperature response $\Delta\overline{T}_X$ increases eastward from the western boundary X_{W} and reaches a maximum $\Delta\overline{T}_{\mathrm{max}}$ at the longitude $X_{\Delta\overline{T}_{\mathrm{max}}}$ where the anomalous vertical motion switches sign (from enhanced sinking to enhanced rising). From the longitude $X_{\Delta\overline{T}_{\mathrm{max}}}$, $\Delta\overline{T}_X$ decreases eastward due to the enhanced rising motion over the eastern extratropical North Pacific. Hence, the maximum warming response $\Delta\overline{T}_{\mathrm{max}}$ (Figs. 4, 6, 7b) is located at the longitude $X_{\Delta\overline{T}_{\mathrm{max}}}$ where the anomalous vertical motion switches sign. A positive heat flux anomaly ($\overline{U}_{RDC}\Delta\overline{T}_{\mathrm{max}}>0$) is transported eastward by the mean zonal wind across the longitude $X_{\Delta\overline{T}_{\mathrm{max}}}$, providing a negative (positive) feedback to the warm temperature response over the western (eastern) extratropical North Pacific.

Over the tropical/subtropical North Pacific at 200hPa, the climatology of $\frac{\partial\overline{\theta}_{\mathrm{RDC}}}{\partial p}$ (below the tropopause) is much smaller, thus the term $-\Delta\overline{\omega}\frac{\partial\overline{\theta}_{\mathrm{RDC}}}{\partial p}\left(\frac{p}{p_s}\right)^{\frac{R_d}{c_p}}$ is much smaller (Fig. 7b) even there is significant change in the vertical motion (Fig. 6) over the tropical/subtropical North Pacific at 200hPa. Consistently, the term $-\overline{u}_{\mathrm{RDC}}\frac{\partial\Delta\overline{T}}{\partial x}$ (Fig. 7a) and associated temperature response (Fig. 4a)

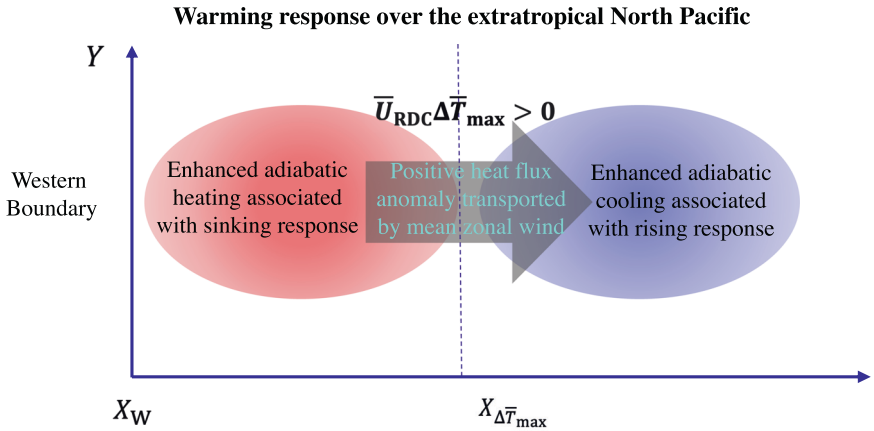

Fig. 8 Schematic relating the temperature anomaly to the adiabatic heating anomaly at upper troposphere/lower stratosphere over the extratropical North Pacific. Over the extratropical North Pacific, the sinking (rising) response results in enhanced adiabatic heating (cooling) over the sinking (rising) region. The integrated enhanced adiabatic heating over the western extratropical North Pacific (upstream of the eastward mean zonal wind) increases and induces a warm temperature response $\Delta\overline{T}_X$, which increases eastward from the western boundary X_W and reaches a maximum $\Delta\overline{T}_{max}$ at the longitude $X_{\Delta\overline{T}_{max}}$ where the anomalous vertical motion switches sign (from enhanced sinking to enhanced rising). From the longitude$X_{\Delta\overline{T}_{max}}$, $\Delta\overline{T}_X$ decreases eastward due to the enhanced rising/adiabatic cooling over the eastern extratropical North Pacific. Hence the maximum warming response $\Delta\overline{T}_{max}$ is located at the longitude $X_{\Delta\overline{T}_{max}}$ where the anomalous vertical motion switches sign. A positive heat flux anomaly ($\overline{U}_{RDC}\Delta\overline{T}_{max}>0$) is transported eastward by the mean zonal wind across the longitude $X_{\Delta\overline{T}_{max}}$, providing a negative (positive) feedback to the warm temperature response over the western (eastern) extratropical North Pacific.

are also much smaller over the tropical/subtropical North Pacific at 200hPa. The contrast between the extratropical and subtropical temperature response at the upper troposphere/lower stratosphere contributes to the enhanced jet stream response centered around 32°N over the North Pacific through the thermal wind relationship.

Since the winter upper troposphere/lower stratosphere vertical motion response $\Delta\overline{\omega}$ over the extratropical North Pacific is also affected by the tropical North Pacific ITCZ/Walker circulation response to the North Atlantic biases, the simple relationship between the leading horizontal advection and adiabatic heating terms (Eqs. 1, 2) at 200hPa suggests that the North Atlantic-induced changes in the tropical North Pacific ITCZ/Walker Circulation may play an important role in the winter upper troposphere/lower stratosphere temperature response. As discussed earlier, the difference between the control simulation and the SST Nudging experiments underestimates the North Atlantic cold SST biases, and there is a weaker North Atlantic-induced ITCZ shift/Walker circulation change and thus a weaker vertical motion/warming response in the upper troposphere/lower stratosphere over the extratropical North Pacific for the case "Control-SST Nudging" compared to the case "Control-RDC" (Supplementary Fig. 6). These results support the important role of the North Atlantic-induced Walker circulation changes in influencing the vertical motion and warming response over the extratropical North Pacific. Similarly, a stronger North Atlantic-induced ITCZ/Walker circulation response, which could be amplified by the cloud feedback[56], may contribute to a stronger upper troposphere/lower stratosphere warming temperature response, and thus a stronger jet stream response over the extratropical North Pacific through the thermal wind relationship. In contrast, there is no such winter upper troposphere/lower stratosphere warming temperature response over the extratropical North Atlantic, consistent with the fact that the winter vertical motion response is limited to the middle/lower troposphere over the extratropical North Atlantic.

During winter at lower troposphere (850hPa) over the extratropical North Pacific, changes in the diabatic heating and convergence of horizontal transient eddy heat flux become more important, whereas changes in the adiabatic heating are less important. The cooling response at 850hPa over the western and central extratropical North Pacific is sustained by reduced horizontal advection and damped by enhanced diabatic heating and convergence of horizontal transient eddy heat flux (Supplementary Fig. 10c–e). The dominant thermodynamic terms sustaining the low-level cooling response over the North Pacific and the North Atlantic reveal the contrasting nature between the two basins. Over the extratropical North Atlantic, the low-level cooling response is maintained by the oceanic-induced reduction in air-sea turbulent heat fluxes and associated diabatic heating (Supplementary Figs. 4b, 10d) and damped by atmospheric feedback (i.e., enhanced horizontal advection and transient eddy heat flux convergence) (Supplementary Fig. 10c, e). In contrast, over the extratropical North Pacific, the low-level cooling is sustained by reduced atmospheric horizontal advection (Supplementary Fig. 10c) and damped mainly by enhanced local air-sea turbulent heat fluxes and associated diabatic heating in most regions except the Kuroshio extension (Supplementary Figs. 4b, 10d).

The schematic diagram (Fig. 9a) summarizes the dominant thermodynamic processes that sustain the changes in winter atmospheric temperature over the extratropical North Pacific, as discussed earlier. The cyclonic circulation response and associated vertical dipole atmospheric temperature response can be seen in both zonal and meridional sections averaged over the extratropical North Pacific (Figs. 5a, 9b), despite that the low-level cooling response is concentrated over the western extratropical North Pacific (Fig. 9b). The thermodynamic analysis suggests that reduced horizontal advection sustains the low-level cooling over the western extratropical North Pacific, whereas enhanced horizontal advection damps the low-level cooling over the eastern extratropical North Pacific (Supplementary Fig. 10c). In addition, along the western boundary current pathway and the Kuroshio extension in the extratropical North Pacific, the SST cooling is intensified (Fig. 9a, Supplementary Fig. 4a) due to coupled oceanic response to the enhanced cyclonic atmospheric circulation over the extratropical North Pacific[9]. Hence the local air-sea turbulent heat fluxes (sensible plus latent heat fluxes) are reduced along the Kuroshio extension (Supplementary Fig. 4b), contributing to the enhanced low-level cooling above through coupled air-sea interactions.

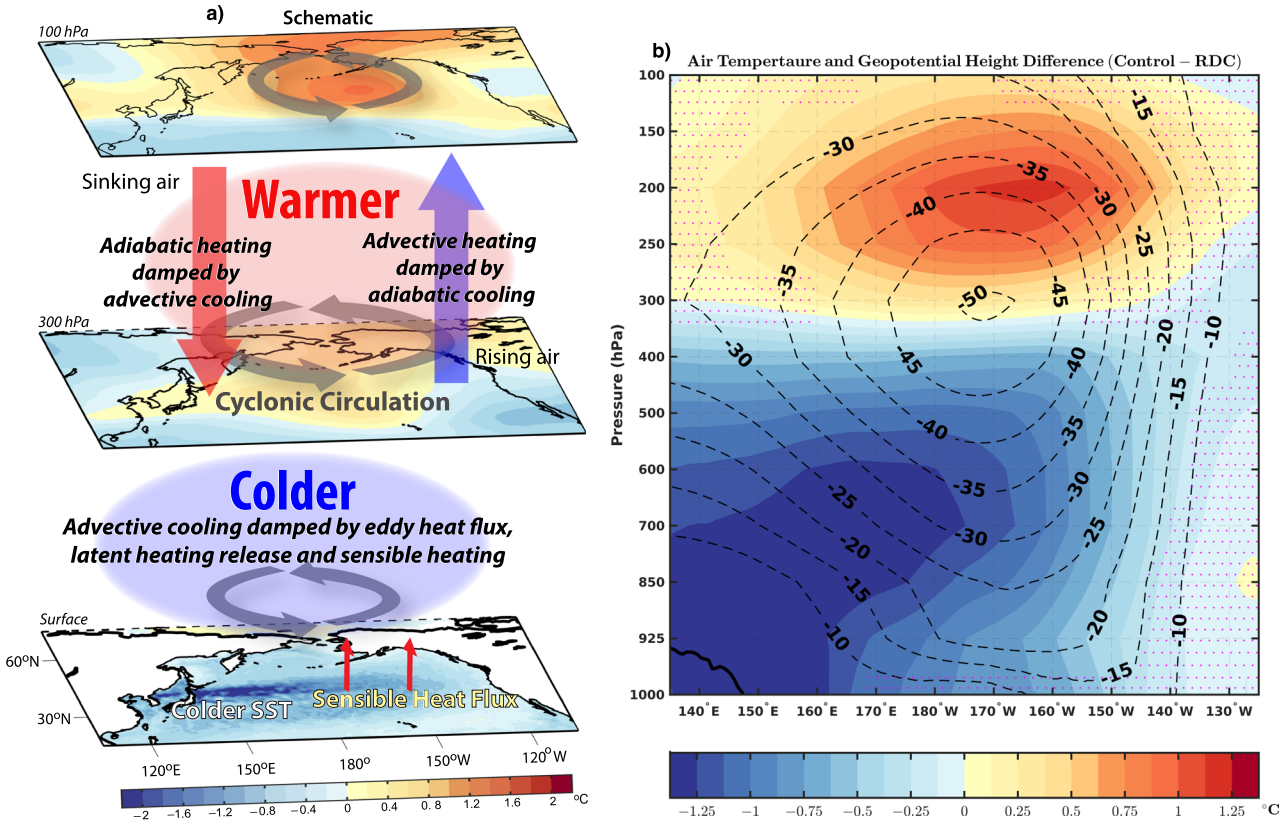

Fig. 9 Schematic of the thermodynamic process sustaining warming at upper troposphere/lower stratosphere and cooling at middle/lower troposphere and meridional averaged winter (JFM) mean temperature (geopotential height) response over the extratropical North Pacific in response to the North Atlantic biases. a Schematic over the extratropical North Pacific. At the lower troposphere, the cooling response over the western and central extratropical North Pacific (blue shading) is sustained by reduced horizontal advection. The enhanced convergence of eddy heat flux, latent heating release, and sensible heat flux (red arrows at the surface) tend to damp it. In the upper troposphere/lower stratosphere, the warming response (red shading) is sustained by enhanced adiabatic (horizontal advective) heating and damped by enhanced horizontal advective (adiabatic) cooling over the western (eastern) extratropical North Pacific. The sinking (rising) response associated with the enhanced adiabatic heating (cooling) is represented as red (blue) arrow. **b** Meridional averaged temperature (geopotential height) response (Control -RDC) in °C (m) between 30°N and 55°N over the North Pacific, represented as color (contour). The horizontal circulation response revealed by the geopotential height is cyclonic and has a maximum at approximately 300hPa where the temperature response switches sign. Stippling (magenta color) here represents the region where differences are not significant at 5% level.

DISCUSSION

In this study, we employ the RDC approach to focus on the remote impacts of the North Atlantic biases on winter upper troposphere/lower stratosphere temperature/vertical motion response over the extratropical North Pacific. The RDC approach provides a realistic North Atlantic ocean circulation and effectively corrects the North Atlantic SST biases simulated by the coupled model. Our results suggest that during wintertime, the North Atlantic biases lead to a warmer upper troposphere/lower stratosphere temperature, in addition to the colder middle and lower tropospheric temperature over the extratropical North Pacific. We discuss the thermodynamic mechanisms sustaining the winter vertical dipole atmospheric temperature response over the extratropical North Pacific. The vertical level at which the dipole atmospheric temperature change switches sign is also the vertical level of the maximum change in the geopotential height. Therefore, understanding the unexplored winter upper troposphere/lower stratosphere temperature response is important for understanding the maximum jet stream response over the extratropical North Pacific through the thermal wind relationship. Many previous studies on the Atlantic-Pacific teleconnection are focused on the horizontal circulation and associated SST/lower troposphere temperature response over the North Pacific[9–11,14,19–21,33–37]. Here we investigate the unexplored winter upper troposphere/lower stratosphere temperature response over the extratropical North Pacific.

Our thermodynamic analysis suggests that the wintertime low-level cooling response over the western and central extratropical North Pacific is associated with reduced horizontal advection. The wintertime upper troposphere/lower stratosphere warming response is associated with changes in the upper troposphere/lower stratosphere adiabatic heating and horizontal advection over the extratropical North Pacific. Changes in the upper troposphere/lower stratosphere vertical velocity dominate changes in the upper troposphere/lower stratosphere adiabatic heating over the extratropical North Pacific and are affected by the tropical North Pacific ITCZ/Walker circulation response induced by the North Atlantic biases. The wintertime atmospheric temperature and velocity changes over the North Pacific are closely coupled to each other to sustain a coherent response.

Our thermodynamic analysis reveals a simple leading order relationship in the upper troposphere/lower stratosphere between the mean zonal flow advection of the temperature change $(-\overline{u}_{\mathrm{RDC}}\frac{\partial\Delta\overline{T}}{\partial x})$ and the vertical advection of the mean potential temperature by the change in vertical velocity $\left(-\Delta\overline{\omega}\frac{\partial\overline{\theta}_{\mathrm{RDC}}}{\partial p}\left(\frac{p}{p_s}\right)^{\frac{R_d}{c_p}}\right)$ over the extratropical North Pacific. With the known mean fields and if the change in vertical velocity is given, this simple and powerful relationship in the upper troposphere/lower stratosphere can provide a rough estimation of the upper troposphere/

lower stratosphere temperature response over the extratropical North Pacific. In the upper troposphere/lower stratosphere, with an integrated increase in the sinking vertical motion/adiabatic heating over the western extratropical North Pacific, the warm temperature response increases eastward and reaches a maximum at the longitude where the anomalous vertical motion switches sign (from enhanced sinking to enhanced rising). This simple leading order relationship also suggests that a stronger North Atlantic-induced ITCZ/Walker circulation response may contribute to a stronger upper troposphere/lower stratosphere warming temperature response and, thus a stronger jet stream response over the extratropical North Pacific through the thermal wind relationship.

The vertical velocity changes in the upper troposphere/lower stratosphere associated with changes in the upper troposphere/lower stratosphere convergence/divergence over the western/eastern extratropical North Pacific reflect the remarkable wintertime impacts that the North Atlantic biases can have at remote locations. In contrast, the local changes in winter vertical velocity over the extratropical western North Atlantic in response to modeled biases in the North Atlantic western boundary current (Gulf Stream and North Atlantic Current) are mainly confined to the marine boundary layer in the lower and middle troposphere, consistent with previous studies[45,47]. Hence the North Atlantic ocean circulation biases and associated SST biases can have sustained influence on remote upper troposphere/lower stratosphere vertical motion over the extratropical North Pacific even if their climatic impacts on local tropospheric vertical motion over the extratropical North Atlantic are shallow in winter. The lack of significant upper troposphere/lower stratosphere warming response over the extratropical North Atlantic is consistent with the lack of vertical motion and associated adiabatic heating response over this region.

Previous studies suggest that coupled ocean-atmosphere interactions can provide positive feedback over the extratropical North Pacific, reinforcing the near-surface cooling response over this region[9,57]. The strengthened lower-level response could contribute to a stronger upper-level negative geopotential height response through hydrostatic balance and enhance the upper-level convergence/sinking motion over the western extratropical North Pacific, and thus contribute to a stronger upper-level warming response over the extratropical North Pacific. Other potential pathways for the North Atlantic-induced North Pacific response could also exist. For example, one notable pathway is the oceanic teleconnection through the Bering Strait, where the anomalous freshwater forcing in the subarctic North Atlantic could result in the transport of colder water from the Arctic into the North Pacific through Bering Strait, causing a colder extratropical North Pacific SST[19]. Another possible pathway is through the response in the Arctic sea ice. The Arctic sea ice change induced by the change in the North Atlantic ocean circulation and heat transport[58–60] could possibly affect air temperature and mid-latitude jet stream over the extratropical North Pacific[61].

Our results here provide a deeper understanding of the winter atmospheric response over the extratropical North Pacific to the North Atlantic biases and help bridge the gap in our current knowledge. The North Atlantic biases also lead to an increase in the large-scale extreme precipitation over the western United States by ~30–40%, in association with a southward shift of the storm track over both the North Atlantic and the North Pacific, suggesting the profound remote societal impact that changes in the North Atlantic ocean circulation could have. It is likely that the amplitude of the North Atlantic-induced response over both the tropical and the extratropical North Pacific and associated coupled air-sea interactions are underestimated in climate models[9,21]. The vertical dipole atmospheric temperature anomaly over the extratropical North Pacific associated with the observed PDO[31,32] resembles the spatial pattern of the winter atmospheric response found in this study. Given the potential socioeconomic impacts, a better understanding of the winter temperature and associated jet stream changes over the extratropical North Pacific in response to changes in the North Atlantic is of great importance. In particular, more investigations need to be conducted to assess the remote impacts of future North Atlantic changes on winter atmospheric temperature and associated jet stream response over the extratropical North Pacific.

METHODS

Robust diagnostic calculations (RDC) and sea surface temperature (SST) nudging

The RDC approach used here is similar to that used by Zhang and Thomas[54]. In the RDC experiment used in this study, the North Atlantic potential temperature and salinity in a fully coupled high-resolution climate model (described below) are restored to the observed hydrographic climatology in the entire ocean column to produce a realistic North Atlantic ocean circulation, thus correcting the North Atlantic ocean circulation and associated SST biases. The restoring region in the North Atlantic is between 15°N and 65°N. The restoring timescale is 5 days in the extratropical North Atlantic (30°N – 60°N) and 180 days in the buffer zones (subtropical North Atlantic [15°N – 30°N] and sub-polar North Atlantic [60°N-65°N]). Outside the North Atlantic restoring region, the ocean is free to evolve except in the Arctic Mediterranean region (90°W to 60°E and 65°N to 80°N), where the potential temperature and salinity in the entire ocean column is restored to the control simulation climatology with a 5-day restoring timescale to avoid any oceanic impacts of the RDC over the Arctic Mediterranean region. We use the Commonwealth Scientific and Industrial Research Organisation (CSIRO) ATLAS of REGIONAL SEAS 2009 version (CARS2009)[62,63] combined with the World Ocean Atlas 2013 (WOA13) version 2[64,65] as the observed hydrographic climatology for the RDC experiment (See Zhang & Thomas, 2021[54] for details).

In the SST nudging experiment, only the North Atlantic SST in the fully coupled high-resolution climate model is restored to observed climatological data. Without restoring the subsurface temperature/salinity to the observed hydrographic climatology, the modeled North Atlantic ocean circulation remains biased and unrealistic in the SST nudging experiment. The restoring region and restoring time scale for the North Atlantic SST are the same as the RDC experiment. Outside the North Atlantic restoring region, the ocean is free to evolve except in the Arctic Mediterranean region (90°W to 60°E and 65°N to 80°N), where the potential temperature and salinity in the entire column is restored to the control simulation climatology as done in the RDC experiment to avoid any oceanic impacts of the SST nudging over the Arctic Mediterranean region. Both the SST nudging and RDC experiments are conducted for 80 years. To avoid the initial spin-up, we use the last 60 years of data (year 21 to 80) of the SST nudging and RDC experiments for our analysis. The atmospheric outputs used for diagnosing eddy fluxes are saved for every 6 h. For the frequently used SST nudging approach[15,66] in the fully coupled model, simply restoring the North Atlantic SST to the observed climatology without correcting the North Atlantic ocean circulation leads to an inconsistent situation, and thus, it is less effective in correcting the North Atlantic SST biases than the RDC approach with the same restoring time scale.

Coupled climate model and control simulation

For this study, we use the Geophysical Fluid Dynamics Laboratory (GFDL) coupled climate model version 2.5 (CM2.5)[48]. CM2.5 is a high-resolution fully coupled global climate model with a horizontal resolution of ~0.5° in the atmosphere and ~0.25° in the ocean. We use a constant 1990 radiative forcing for the control

simulation. The same radiative forcing was used for the RDC and SST nudging experiments as well. To compare with the RDC and SST nudging experiments, we use the corresponding 60 years of data (year 21 to 80) of the control simulation for our analysis. The atmospheric outputs used for diagnosing eddy fluxes are saved for every 6 h. The 60-year long-term mean difference between the control and RDC experiments (Control minus RDC) is used to assess the influence of the North Atlantic biases on winter atmospheric change over the North Pacific. We use the two-sided student t-test for the statistical testing of the 60-year long-term mean wintertime difference between the control and RDC experiments.

Thermodynamic analysis

For our thermodynamic analysis, we use the following approach that is similar to one proposed by Li et al.[55] to study the vertical dipole atmospheric temperature anomaly over the Tibetan Plateau. The thermodynamic energy equation (Holton, 2004[67]) is

$$\frac{DT}{Dt} = \frac{1}{c_p \rho}\frac{Dp}{Dt} + \frac{\dot{Q}}{c_p} \tag{4}$$

where T is the temperature, c_p is the heat capacity of air at constant pressure, ρ is density, p is the pressure. Here $\dot{Q}$ is the diabatic heating rate per unit mass and can be decomposed into $\dot{Q}_{SW}, \dot{Q}_{LW}, \dot{Q}_L$ and $\dot{Q}_S$, i.e., the contribution to the diabatic heating rate from shortwave radiation, longwave radiation, latent heating release and sensible heating respectively. The contribution from surface boundary layer dissipative heating is negligible. In isobaric coordinates, $\frac{Dp}{Dt} = \omega$, where ω is the vertical velocity. Introducing potential temperature $\theta = T\left(\frac{p_s}{p}\right)^{\frac{R_d}{c_p}}$ (here p_s is the surface pressure) and using the ideal gas law, we can simplify Eq. (4) to get

$$\frac{\partial T}{\partial t} = -\mathbf{u}.\nabla T - \omega\frac{\partial \theta}{\partial p}\left(\frac{p}{p_s}\right)^{\frac{R_d}{c_p}} + \frac{\dot{Q}}{c_p} \tag{5}$$

We use the above form of the thermodynamic energy equation for our analysis. The variable X (temperature or velocity) in the thermodynamic energy equation can be thought to be the sum of temporal mean (denoted as overbar) and anomaly (denoted as prime) deviated from temporal mean. For instance, temperature can be written as $T = \overline{T} + T'$. Noting that mean and anomaly velocity field under Boussinesq approximation satisfies the continuity equation we get

$$\frac{\partial \overline{T}}{\partial t} = -\overline{\mathbf{u}}.\nabla \overline{T} - \overline{\omega}\frac{\partial \overline{\theta}}{\partial p}\left(\frac{p}{p_s}\right)^{\frac{R_d}{c_p}} - \nabla.(\overline{\mathbf{u}'T'}) - \frac{\partial \overline{\omega'\theta'}}{\partial p}\left(\frac{p}{p_s}\right)^{\frac{R_d}{c_p}} + \frac{\overline{\dot{Q}}}{c_p} \tag{6}$$

For time averaging over a long period, $\frac{\partial \overline{T}}{\partial t}$ is negligible. Hence, we have,

$$0 \approx -\overline{\mathbf{u}}.\nabla \overline{T} - \overline{\omega}\frac{\partial \overline{\theta}}{\partial p}\left(\frac{p}{p_s}\right)^{\frac{R_d}{c_p}} - \nabla.(\overline{\mathbf{u}'T'}) - \frac{\partial \overline{\omega'\theta'}}{\partial p}\left(\frac{p}{p_s}\right)^{\frac{R_d}{c_p}} + \frac{\overline{\dot{Q}}}{c_p} \tag{7}$$

The above equation is for the thermal equilibrium state of the atmosphere, where $-\overline{\mathbf{u}}.\nabla\overline{T}$ is the horizontal advection, $-\overline{\omega}\frac{\partial\overline{\theta}}{\partial p}\left(\frac{p}{p_s}\right)^{\frac{R_d}{c_p}}$ is referred to as the adiabatic heating term[55] (which is related to the vertical advection of the potential temperature), $-\nabla.(\overline{\mathbf{u}'T'})$ denotes the horizontal eddy heat flux convergence, $-\frac{\partial\overline{\omega'\theta'}}{\partial p}\left(\frac{p}{p_s}\right)^{\frac{R_d}{c_p}}$ represents the sum of the vertical eddy heat flux convergence and the transient adiabatic heating, and the final term $\frac{\overline{\dot{Q}}}{c_p}$ represents the diabatic heating.

We modify the above equation and define Δ as the difference between the Control and RDC experiments for the terms in above equation:

$$0 \approx \Delta(-\overline{\mathbf{u}}.\nabla\overline{T}) + \Delta\left(-\overline{\omega}\frac{\partial\overline{\theta}}{\partial p}\left(\frac{p}{p_s}\right)^{\frac{R_d}{c_p}}\right) + \Delta(-\nabla.(\overline{\mathbf{u}'T'})) + \Delta\left(-\frac{\partial\overline{\omega'\theta'}}{\partial p}\left(\frac{p}{p_s}\right)^{\frac{R_d}{c_p}}\right) + \Delta\left(\frac{\overline{\dot{Q}}}{c_p}\right) \tag{8}$$

We use the above equation for the thermodynamic analysis, similar to the approach discussed by Li et al.[55] based on non-transient disturbances. Here we use the thermodynamic equation that includes contributions from both transient and non-transient disturbances since the role of horizontal transient eddy heat flux convergence in the midlatitudes (especially at lower troposphere) cannot be neglected in winter. A positive (negative) value of Δ in any term here on the right hand side (RHS) indicates a contribution in increasing (decreasing) the temperature. The sum of the individual terms on the RHS of the above thermodynamic equation is approximately zero, i.e., the total heat budget is closed.

Contribution from terms involving difference in long-term mean temperature and/or velocity

The difference in the non-transient term in the thermodynamic analysis can be expressed as combinations of terms involving differences in long-term mean velocity and/or long-term mean temperature between the two experiments. So, we can rewrite the difference in the horizontal temperature advection term (first RHS term in Eq. 8) as:

$$\begin{aligned}\Delta(-\overline{\mathbf{u}}.\nabla\overline{T}) &= (-\overline{\mathbf{u}}.\nabla\overline{T})_{Con} - (-\overline{\mathbf{u}}.\nabla\overline{T})_{RDC} \\ &= -\overline{u}_{RDC}\frac{\partial\Delta\overline{T}}{\partial x} - \overline{v}_{RDC}\frac{\partial\Delta\overline{T}}{\partial y} - \Delta\overline{u}\frac{\partial\overline{T}_{RDC}}{\partial x} \\ &\quad - \Delta\overline{v}\frac{\partial\overline{T}_{RDC}}{\partial y} - \Delta\overline{u}\frac{\partial\Delta\overline{T}}{\partial x} - \Delta\overline{v}\frac{\partial\Delta\overline{T}}{\partial y}\end{aligned} \tag{9}$$

where subscript Con and RDC denotes control and RDC experiments and Δ denotes the long-term mean wintertime difference between control and RDC experiments. The first two terms on the final RHS of Eq. (9) denote the contribution of the horizontal advection by the mean flow of the difference in temperature. The next two terms denote the contribution of the horizontal advection by the difference in winds of the mean temperature. The last two terms indicate the contribution of the horizontal advection by the difference in winds of the difference in temperature. Using Eq. (9) we can assess which individual component on the RHS dominated the total difference on the left hand side of the equation.

Similarly, the second term (difference in adiabatic heating) on the RHS of Eq. (8) can be written as combinations of terms involving mean and difference in temperature and vertical velocity:

$$\begin{aligned}\Delta\left(-\overline{\omega}\frac{\partial\overline{\theta}}{\partial p}\left(\frac{p}{p_s}\right)^{\frac{R_d}{c_p}}\right) &= \left(-\overline{\omega}\frac{\partial\overline{\theta}}{\partial p}\left(\frac{p}{p_s}\right)^{\frac{R_d}{c_p}}\right)_{Con} - \left(-\overline{\omega}\frac{\partial\overline{\theta}}{\partial p}\left(\frac{p}{p_s}\right)^{\frac{R_d}{c_p}}\right)_{RDC} \\ &= -\left(\overline{\omega}_{RDC}\frac{\partial\Delta\overline{\theta}}{\partial p} + \Delta\overline{\omega}\frac{\partial\overline{\theta}_{RDC}}{\partial p} + \Delta\overline{\omega}\frac{\partial\Delta\overline{\theta}}{\partial p}\right)\left(\frac{p}{p_s}\right)^{\frac{R_d}{c_p}}\end{aligned} \tag{10}$$

DATA AVAILABILITY

The World Ocean Atlas 2013 (WOA13) data were downloaded from the NOAA National Centers for Environmental Information (formerly the National Oceanographic Data) https://www.nodc.noaa.gov/cgi-bin/OC5/woa13/woa13.pl. The CSIRO ATLAS of REGIONAL SEAS 2009 version (CARS2009) data (http://www.marine.csiro.au/~dunn/cars2009/) were developed and provided by the Commonwealth Scientific and Industrial Research Organisation (CSIRO) Marine and Atmospheric Research, and downloaded from http://www.marine.csiro.au/atlas/. The Japanese Ocean Flux Data set with Use of Remote Sensing Observations (J-OFURO3 V1[68]) is for the time period 1988–2013 and can be downloaded from https://www.j-ofuro.com/en/dataset. Other key data used in this study is available from https://doi.org/10.5281/zenodo.8330018[69].

CODE AVAILABILITY

The code of the Geophysical Fluid Dynamics Laboratory (GFDL) coupled climate model version 2.5 (CM2.5) is publicly available at https://www.gfdl.noaa.gov/cm2-5-and-flor-quickstart/.

Received: 29 May 2023; Accepted: 14 September 2023;
Published online: 26 September 2023

REFERENCES

1. Broecker, W. S., Peteet, D. M. & Rind, D. Does the ocean–atmosphere system have more than one stable mode of operation? *Nature* **315**, 21–26 (1985).
2. Cheng, H. et al. Ice age terminations. *Science* **326**, 248–252 (2009).
3. Clark, P. U., Pisias, N. G., Stocker, T. F. & Weaver, A. J. The role of the thermohaline circulation in abrupt climate change. *Nature* **415**, 863–869 (2002).
4. McManus, J. F., Francois, R., Gherardi, J.-M., Keigwin, L. D. & Brown-Leger, S. Collapse and rapid resumption of Atlantic meridional circulation linked to deglacial climate changes. *Nature* **428**, 834–837 (2004).
5. Rahmstorf, S. Ocean circulation and climate during the past 120,000 years. *Nature* **419**, 207–214 (2002).
6. Zhang, R. et al. A review of the role of the Atlantic meridional overturning circulation in Atlantic multidecadal variability and associated climate impacts. *Rev. Geophys.* **57**, 316–375 (2019).
7. Zhang, R., Delworth, T. L. & Held, I. M. Can the Atlantic Ocean drive the observed multidecadal variability in Northern Hemisphere mean temperature? *Geophys. Res. Lett.* **34**, L02709 (2007).
8. Semenov, V. A. et al. The impact of North Atlantic–Arctic multidecadal variability on Northern Hemisphere surface air temperature. *J. Clim.* **23**, 5668–5677 (2010).
9. Zhang, R. & Delworth, T. L. Impact of the Atlantic Multidecadal Oscillation on North Pacific climate variability. *Geophys. Res. Lett.* **34**, L23708 (2007).
10. Wallace, J. M. & Gutzler, D. S. Teleconnections in the geopotential height field during the Northern Hemisphere winter. *Mon. Weather Rev.* **109**, 784–812 (1981).
11. Ruprich-Robert, Y. et al. Assessing the climate impacts of the observed Atlantic multidecadal variability using the GFDL CM2.1 and NCAR CESM1 global coupled models. *J. Clim.* **30**, 2785–2810 (2017).
12. Leathers, D. J., Yarnal, B. & Palecki, M. A. The Pacific/North American teleconnection pattern and United States climate. Part I: Regional temperature and precipitation associations. *J. Clim.* **4**, 517–528 (1991).
13. Abatzoglou, J. T. Influence of the PNA on declining mountain snowpack in the Western United States. *Int. J. Climatol.* **31**, 1135–1142 (2011).
14. Lyu, K., Yu, J.-Y. & Paek, H. The influences of the Atlantic Multidecadal Oscillation on the mean strength of the North Pacific subtropical high during boreal winter. *J. Clim.* **30**, 411–426 (2017).
15. Zhang, L. & Zhao, C. Processes and mechanisms for the model SST biases in the North Atlantic and North Pacific: A link with the Atlantic meridional overturning circulation. *J. Adv. Model. Earth Syst.* **7**, 739–758 (2015).
16. Mantua, N. J., Hare, S. R., Zhang, Y., Wallace, J. M. & Francis, R. C. A Pacific interdecadal climate oscillation with impacts on salmon production. *Bul. Am. Meteorol. Soc.* **78**, 1069–1080 (1997).
17. Chen, X., Wallace, J. M. & Tung, K.-K. Pairwise-rotated EOFs of global SST. *J. Clim.* **30**, 5473–5489 (2017).
18. Deser, C. et al. ENSO and Pacific decadal variability in the Community Climate System Model version 4. *J. Clim.* **25**, 2622–2651 (2012).
19. Okumura, Y. M., Deser, C., Hu, A., Timmermann, A. & Xie, S.-P. North Pacific climate response to freshwater forcing in the subarctic North Atlantic: Oceanic and atmospheric pathways. *J. Clim.* **22**, 1424–1445 (2009).
20. Wu, L., Li, C., Yang, C. & Xie, S.-P. Global teleconnections in response to a shutdown of the Atlantic Meridional Overturning Circulation. *J. Clim.* **21**, 3002–3019 (2008).
21. Zhang, R. & Delworth, T. L. Simulated tropical response to a substantial weakening of the Atlantic thermohaline circulation. *J. Clim.* **18**, 1853–1860 (2005).
22. Barcikowska, M. J., Knutson, T. R. & Zhang, R. Observed and simulated fingerprints of multidecadal climate variability and their contributions to periods of global SST stagnation. *J. Clim.* **30**, 721–737 (2017).
23. Dong, B., Sutton, R. T. & Scaife, A. A. Multidecadal modulation of El Niño–Southern Oscillation (ENSO) variance by Atlantic ocean sea surface temperatures. *Geophys. Res. Lett.* **33**, L08705 (2006).
24. Kucharski, F. et al. Atlantic forcing of Pacific decadal variability. *Clim. Dyn.* **46**, 2337–2351 (2016).
25. Li, X., Xie, S.-P., Gille, S. T. & Yoo, C. Atlantic-induced pan-tropical climate change over the past three decades. *Nat. Clim. Change* **6**, 275–279 (2016).
26. McGregor, S. et al. Recent Walker circulation strengthening and Pacific cooling amplified by Atlantic warming. *Nat. Clim. Change* **4**, 888–892 (2014).
27. Sun, C. et al. Western tropical Pacific Multidecadal variability forced by the Atlantic Multidecadal Oscillation. *Nat. Commun.* **8**, 15998 (2017).
28. Dong, B.-W. & Sutton, R. T. Adjustment of the coupled ocean-atmosphere system to a sudden change in the thermohaline circulation. *Geophys. Res. Lett.* **29**, (2002).
29. Chikamoto, Y., Kimoto, M., Watanabe, M., Ishii, M. & Mochizuki, T. Relationship between the Pacific and Atlantic stepwise climate change during the 1990s. *Geophys. Res. Lett.* **39**, L21710 (2012).
30. Chikamoto, Y. et al. Skilful multi-year predictions of tropical trans-basin climate variability. *Nat. Commun.* **6**, 6869 (2015).
31. Fang, J. & Yang, X.-Q. Structure and dynamics of decadal anomalies in the wintertime midlatitude North Pacific ocean–atmosphere system. *Clim. Dyn.* **47**, 1989–2007 (2016).
32. Tao, L., Yang, X.-Q., Fang, J. & Sun, X. PDO-related wintertime atmospheric anomalies over the midlatitude North Pacific: Local versus remote SST forcing. *J. Clim.* **33**, 6989–7010 (2020).
33. d'Orgeville, M. & Peltier, W. R. On the Pacific Decadal Oscillation and the Atlantic Multidecadal Oscillation: Might they be related? *Geophys. Res. Lett.* **34**, L23705 (2007).
34. Wu, S., Liu, Z., Zhang, R. & Delworth, T. L. On the observed relationship between the Pacific Decadal Oscillation and the Atlantic Multi-decadal Oscillation. *J. Oceanogr.* **67**, 27–35 (2011).
35. Chylek, P., Dubey, M. K., Lesins, G., Li, J. & Hengartner, N. Imprint of the Atlantic multi-decadal oscillation and Pacific decadal oscillation on southwestern US climate: Past, present, and future. *Clim. Dyn.* **43**, 119–129 (2014).
36. Marini, C. & Frankignoul, C. An attempt to deconstruct the Atlantic Multidecadal Oscillation. *Clim. Dyn.* **43**, 607–625 (2014).
37. Nigam, S., Sengupta, A. & Ruiz-Barradas, A. Atlantic–Pacific links in observed Multidecadal SST variability: Is the Atlantic Multidecadal Oscillation's phase reversal orchestrated by the Pacific Decadal Oscillation? *J. Clim.* **33**, 5479–5505 (2020).
38. Wang, C., Zhang, L., Lee, S.-K., Wu, L. & Mechoso, C. R. A global perspective on CMIP5 climate model biases. *Nat. Clim. Change* **4**, 201–205 (2014).
39. Danabasoglu, G. et al. North Atlantic simulations in coordinated ocean-ice reference experiments phase II (CORE-II). Part I: Mean states. *Ocean Model.* **73**, 76–107 (2014).
40. Wang, H., Legg, S. A. & Hallberg, R. W. Representations of the Nordic seas overflows and their large scale climate impact in coupled models. *Ocean Model.* **86**, 76–92 (2015).
41. Drews, A., Greatbatch, R. J., Ding, H., Latif, M. & Park, W. The use of a flow field correction technique for alleviating the North Atlantic cold bias with application to the Kiel climate model. *Ocean Dyn.* **65**, 1079–1093 (2015).
42. Talandier, C. et al. Improvements of simulated western North Atlantic current system and impacts on the AMOC. *Ocean Model.* **76**, 1–19 (2014).
43. Zhang, R. et al. Sensitivity of the North Atlantic ocean circulation to an abrupt change in the Nordic sea overflow in a high resolution global coupled climate model. *J. Geophys. Res.: Oceans* **116**, C12024 (2011).
44. Keeley, S. P., Sutton, R. T. & Shaffrey, L. C. The impact of North Atlantic sea surface temperature errors on the simulation of North Atlantic European region climate. *Q. J. R. Meteorol. Soc.* **138**, 1774–1783 (2012).
45. Kuwano-Yoshida, A., Minobe, S. & Xie, S.-P. Precipitation response to the Gulf Stream in an atmospheric GCM. *J. Clim.* **23**, 3676–3698 (2010).
46. Minobe, S., Kuwano-Yoshida, A., Komori, N., Xie, S.-P. & Small, R. J. Influence of the Gulf Stream on the troposphere. *Nature* **452**, 206–209 (2008).
47. Minobe, S., Miyashita, M., Kuwano-Yoshida, A., Tokinaga, H. & Xie, S.-P. Atmospheric response to the Gulf Stream: Seasonal variations. *J. Clim.* **23**, 3699–3719 (2010).
48. Delworth, T. L. et al. Simulated climate and climate change in the GFDL CM2.5 high-resolution coupled climate model. *J. Clim.* **25**, 2755–2781 (2012).
49. Sarmiento, J. L. & Bryan, K. An ocean transport model for the North Atlantic. *J. Geophys. Res.: Oceans* **87**, 394–408 (1982).
50. Wright, D. G., Thompson, K. R. & Lu, Y. Assimilating long-term hydrographic information into an eddy-permitting model of the North Atlantic. *J. Geophys. Res.: Oceans* **111**, C09022 (2006).
51. Zhang, R. & Vallis, G. K. The role of bottom vortex stretching on the path of the North Atlantic western boundary current and on the northern recirculation gyre. *J. Phys. Oceanogr.* **37**, 2053–2080 (2007).
52. Lee, S.-K. et al. Global meridional overturning circulation inferred from a data-constrained ocean & sea-ice model. *Geophys. Res. Lett.* **46**, 1521–1530 (2019).
53. Lee, S.-K. et al. Human-induced changes in the global meridional overturning circulation are emerging from the Southern ocean. *Commun. Earth Environ.* **4**, 69 (2023).
54. Zhang, R. & Thomas, M. Horizontal circulation across density surfaces contributes substantially to the long-term mean northern Atlantic Meridional Overturning Circulation. *Commun. Earth Environ.* **2**, 112 (2021).

55. Li, X.-F. et al. Thermodynamic controls of the western Tibetan vortex on Tibetan air temperature. *Clim. Dyn.* **53**, 4267–4290 (2019).
56. Zhang, R., Kang, S. M. & Held, I. M. Sensitivity of climate change induced by the weakening of the Atlantic Meridional Overturning Circulation to cloud feedback. *J. Clim.* **23**, 378–389 (2010).
57. Liu, Z. & Wu, L. Atmospheric response to North Pacific SST: The role of ocean–atmosphere coupling. *J. Clim.* **17**, 1859–1882 (2004).
58. Omrani, N.-E. et al. Coupled stratosphere-troposphere-Atlantic multidecadal oscillation and its importance for near-future climate projection. *npj Clim. Atmos. Sci.* **5**, 59 (2022).
59. Li, D., Zhang, R. & Knutson, T. Comparison of mechanisms for low-frequency variability of summer Arctic sea ice in three coupled models. *J. Clim.* **31**, 1205–1226 (2018).
60. Zhang, R. Mechanisms for low-frequency variability of Summer Arctic sea ice extent. *Proc. Natl Acad. Sci.* **112**, 4570–4575 (2015).
61. Zappa, G., Pithan, F. & Shepherd, T. G. Multimodel evidence for an atmospheric circulation response to Arctic sea ice loss in the CMIP5 future projections. *Geophys. Res. Lett.* **45**, 1011–1019 (2018).
62. Dunn, J. R. & Ridgway, K. R. Mapping Ocean properties in regions of complex topography. *Deep Sea Resh. Part I Oceanogr. Res.* **49**, 591–604 (2002).
63. Ridgway, K. R., Dunn, J. R. & Wilkin, J. L. Ocean interpolation by four-dimensional weighted least squares—Application to the waters around Australia. *J. Atmos. Ocean. Tech.* **19**, 1357–1375 (2002).
64. Locarnini, R. A. et al. World Ocean Atlas 2013, Volume 1: Temperature. S. Levitus, Ed., A. Mishonov Technical Ed.; NOAA Atlas NESDIS **73**, 40 pp. (2013).
65. Zweng, M. M. et al. World Ocean Atlas 2013, Volume 2: Salinity. S. Levitus, Ed., A. Mishonov Technical Ed.; NOAA Atlas NESDIS **74**, 39 pp. (2013).
66. Johnson, N. C. et al. The impact of sea surface temperature biases on North American precipitation in a high-resolution climate model. *J. Clim.* **33**, 2427–2447 (2020).
67. Holton, J. R. in *An Introduction to Dynamic Meteorology* (Elsevier Academic Press, London, 2004).
68. Tomita, H., Hihara, T., Kako, S., Kubota, M. & Kutsuwada, K. An introduction to J-OFURO3, a third-generation Japanese ocean flux data set using remote-sensing observations. *J. Oceanogr.* **75**, 171–194 (2019).
69. Joshi, R. & Zhang, R. Supporting Data for "Impacts of the North Atlantic Biases on the Upper Troposphere/Lower Stratosphere over the Extratropical North Pacific" [Data Set]. Zenodo. https://doi.org/10.5281/zenodo.8330018 (2023).

ACKNOWLEDGEMENTS

Leo Donner, Ming Zhao, and Baoqiang Xiang are acknowledged for their helpful comments and suggestions on this work. We thank Catherine Raphael for illustration support. R. J. is supported by Princeton University Graduate School and CIMES Task II funds for graduate research under award NA18OAR4320123 from the National Oceanic and Atmospheric Administration, U.S. Department of Commerce. R. Z. is supported by GFDL base funding. We acknowledge GFDL resources made available for this research.

AUTHOR CONTRIBUTIONS

R.Z. and R.J. conceived the study and designed the main approaches. R.Z. conducted the numerical experiments. R.J. conducted the analysis of the control, RDC, and SST nudging experiments, including the in-depth thermodynamic analysis. The authors discussed the results/interpretations and wrote the paper together.

COMPETING INTERESTS

The authors declare no competing interests.

ADDITIONAL INFORMATION

Supplementary information The online version contains supplementary material available at https://doi.org/10.1038/s41612-023-00482-4.

Correspondence and requests for materials should be addressed to Rajat Joshi or Rong Zhang.

Reprints and permission information is available at http://www.nature.com/reprints

Publisher's note Springer Nature remains neutral with regard to jurisdictional claims in published maps and institutional affiliations.